Pergamon

Solid-State Electronics Vol. 42, No. 1, pp. 79–85, 1998

Printed in Great Britain

PII: S0038-1101(97)00196-2

0038-1101/98 $19.00 + 0.00

NOISE ANALYSIS OF 0.1 μm GATE MESFETs AND HEMTs

JAVIER MATEOS[1], TOMÁS GONZÁLEZ[1], DANIEL PARDO[1], PATRICK TADYSZAK[2], FRANÇOIS DANNEVILLE[2] and ALAIN CAPPY[2]

[1]Departamento de Física Aplicada, Universidad de Salamanca. Plaza de la Merced s/n, 37008 Salamanca, Spain; [2]Institut d'Electronique et Microélectronique du Nord U.M.R. C.N.R.S. no. 9929 Département Hyperfréquences et Semiconducteurs, BP 69, 59652 Villeneuve D'Ascq Cédex, France

(Received 24 March 1997; in revised form 27 May 1997)

Abstract—Using a semiclassical 2D Monte-Carlo simulation we analyse the noise behaviour of 0.1 μm recessed gate GaAs MESFET and AlGaAs/GaAs HEMT structures. The first step in the noise characterisation is the calculation of the intrinsic small signal equivalent circuit of these devices. Next, by first time using Monte Carlo simulations, the P, R and C noise parameters of both structures are evaluated, and their dependence on bias is analysed. It is found that short-channel effects are more important in the MESFET than in the HEMT. The most significant difference between both devices is that the maximum of the transconductance in the HEMT appears at a lower drain current than in the MESFET. Therefore, even if both structures show similar noise performance in terms of P, R and C noise parameters, the optimum operation point of the HEMT takes place at lower gate voltages, where its noise behaviour is better. As a consequence, the intrinsic minimum noise figure for the HEMT reaches a value as low as 2.5 dB at 100 GHz, while it is higher in the case of the MESFET, with a value of 5.5 dB.

PACS numbers: 72.70. + m, 85.30.Tv, 85.30.De

1. INTRODUCTION

When comparing high electron mobility transistors (HEMTs) with the usual field effect transistors (MESFETs), it is found that heterojunction devices have reached better noise performance at higher frequencies[1–3]. Just after the fabrication of the first HEMT[4], it was believed that the effect of the two-dimensional electron gas (2DEG) was responsible for this better behaviour. But in recent years HEMT and MESFET structures have shown similar cut-off frequencies, f_t, and noise figures[5]. In Ref. [5] it is demonstrated, by means of a study of the temperature dependence of these parameters, that the 2DEG is not the cause of the usually better performance of the heterojunction devices. In fact the properties of the devices are only related to their material composition (regardless of the existence or not of a heterojunction). However, the higher electron mobility in the HEMT provides a larger transconductance (as pointed out in [6]). This fact, together with the lower influence of the parasitic capacitances, usually makes f_t higher in HEMTs. In addition, the aspect ratio (L_g/A, gate length over layer thickness) is usually larger in HEMTs, and consequently the same occurs with the correlation coefficient C. This leads to a stronger cancellation between the drain- and gate-current noise sources, and hence to a lower noise figure.

Here we further investigate the microscopic processes taking place in the two types of devices, their differences and the effect they may have on the measured noise. To this aim Monte Carlo simulation[7] of a recessed GaAs MESFET and a recessed GaAs/AlGaAs HEMT is carried out. The validity of the approach is well contrasted by comparison of the results obtained from the simulation with experimental measurements of static I–V characteristics and noise temperature of the same recessed structures before the gate is fabricated, which was reported in Refs [8,9]. The geometries chosen for the MESFET and HEMT structures are the same as those analysed in these previous studies and they are not optimised to reach the best possible performance. In particular, the aspect ratio of the simulated devices is lower than usual. In order to avoid short-channel effects, commercial MESFETs and HEMTs present higher values of aspect ratio. Therefore, these negative effects will appear in our devices and it will be possible to study their different influence on both kind of structures. Furthermore the aspect ratio in real HEMTs is usually higher than in real MESFETs, a feature which was also considered in the choice of the simulated geometries. So, even when the comparison performed is not the most general one, it can give us important information on the different microscopic processes taking place in both kind of structures and the consequences on their macroscopic behaviour.

The noise characterisation begins with the calculation of the parameters of the intrinsic small signal equivalent circuit. Then the P, R and C noise

parameters are calculated, and their dependence on bias is determined for both devices. To our knowledge, this is the first time these parameters are calculated for MESFETs and HEMTs by using the Monte Carlo method. Even if the precision for the R and C parameters (related to the gate–current noise and drain–gate correlation, respectively) is not very high, their values are an indicator of the qualitative noise behaviour of the devices, and they are very useful to compare the noise performance of different structures.

In Section 2 the details of the Monte Carlo simulation and the theoretical basis of the calculations will be given. Section 3 presents the main results, and finally Section 4 presents the principal conclusions of our work.

2. MONTE CARLO SIMULATION

A semiclassical ensemble Monte Carlo simulator coupled with a two-dimensional Poisson solver is used for the analysis of the devices. It will not be considered neither the quantization of energy levels in the 2DEG, nor the quantum reflection or tunnelling through the barrier at the heterojunction (classical laws of conservation of energy and momentum perpendicular to the heterojunction are used). The only quantum effect taken into account is the Pauli exclusion principle[10]. This physical model used for the simulation of HEMTs was already demonstrated to provide correct results[11–14]. Ohmic boundary conditions[15] are considered at the drain and source contacts, with non-uniform profile of potential and electron concentration in the case of the HEMT (as if real top electrodes were used)[9,16]. The gate Schottky contact allows carriers to leave the device, but it does not inject them. The temperature is 300 K. Other details of the simulation can be found elsewhere[8,9,17,18].

The diagrams of the simulated HEMT and MESFET are shown in Fig. 1. The geometries and dopings of the structures are the same as those used to reproduce the behaviour of the fabricated ungated devices[8,9]. The recess depths were adjusted in such a way that both ungated structures gave similar levels of current[9]. The aspect ratio is quite low, 2.0 for the MESFET and 3.6 for the HEMT, while in usual devices it is higher than 5 to avoid short-channel effects. Therefore, these undesirable effects, which could be eluded by means of an adequate design, will degrade the performance of our devices, and it will be possible to analyse their consequences. The abrupt recess geometry is the same as that of the real ungated structures and results from the high anisotropy of the plasma etching, thus drawing a rectangular shape in the surface of the device. The effect of the surface potential on the three walls of the recess has been taken into account through a static charge (shown as a dotted line in Fig. 1)[8,19].

The intrinsic equivalent circuit commonly used for MESFETs[20] is also valid and applied here for HEMTs[21,22]. It reflects appropriately the small signal behaviour of both kind of devices and allows the comparison between them. The method for calculating the parameters of this small signal equivalent circuit was described in [20]. It is based on the calculation of the Y parameters through the Fourier analysis of the transient behaviour of the device when a voltage step is applied to the gate or drain electrode. From these Y parameters the values of the different elements of the intrinsic equivalent circuit are extracted: the gate–drain, gate–source and drain–source capacitances, C_{gd}, C_{gs} and C_{ds}, respectively, the transconductance, g_m, the drain conductance, g_{ds}, the channel resistance between source and gate, R_i, and the delay time, τ.

The noise characterisation requires firstly the calculation of the spectral densities of the drain- and gate–current fluctuations and its cross-correlation, S_{i_d}, S_{i_g} and $S_{i_g i_d}$, respectively, which is performed following Ref. [23]. Then the intrinsic dimensionless noise parameters P, R and C are determined as follows[6,22,24–27]:

$$P = \frac{S_{i_d}}{4K_B T_a |Y_{21}|} \tag{1}$$

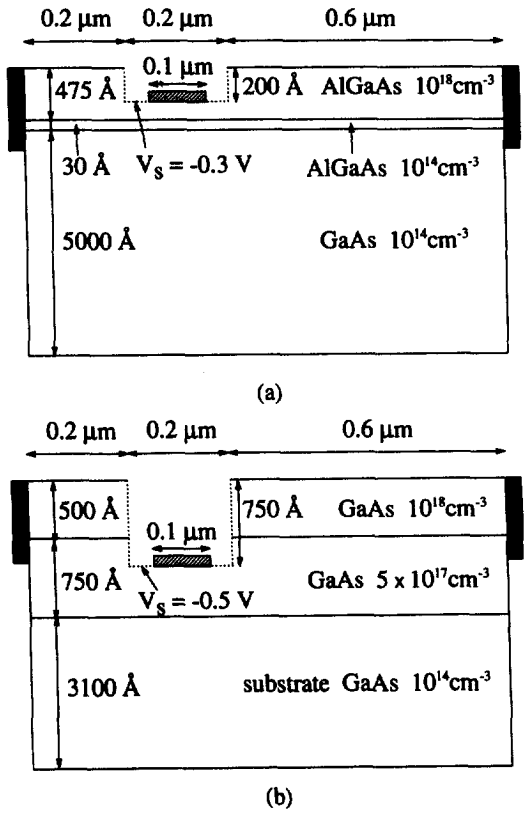

Fig. 1. Scheme of the simulated devices; (a) HEMT, (b) MESFET.

$$R = \frac{S_{i_g} |Y_{21}|}{4K_B T_a |Y_{11}|^2} \tag{2}$$

$$C = \frac{\mathrm{Im}[S_{i_g i_d}]}{\sqrt{S_{i_g} S_{i_d}}} \tag{3}$$

where K_B is the Boltzmann constant and T_a the ambient temperature.

Another important parameter for the noise characterisation of the devices is the noise figure. The intrinsic minimum noise figure, F_{int}, can be calculated exactly by using the following formulas[28–30];

$$F_{int} = 1 + 2R_n(G_{cor} + G_{opt}) \tag{4}$$

with;

$$R_n = \frac{S_{i_d}}{4K_B T_a |Y_{21}|^2} \tag{5}$$

$$G_{cor} = \mathrm{Re}\left[Y_{11} - Y_{21} \frac{S^*_{i_g i_d}}{S_{i_d}} \right] \tag{6}$$

$$A = |Y_{21}|^2 \frac{S_{i_g}}{S_{i_d}} + |Y_{11}|^2 - 2\mathrm{Re}\left[Y_{11} Y^*_{21} \frac{S_{i_g i_d}}{S_{i_d}} \right] \tag{7}$$

$$B = \left[\mathrm{Im}\left[Y_{11} + Y^*_{21} \frac{S_{i_g i_d}}{S_{i_d}} \right] \right]^2 \tag{8}$$

$$G_{opt} = \sqrt{A - B} \tag{9}$$

where *, Re and Im stand for complex conjugate, real part and imaginary part, respectively, of the corresponding complex magnitude. The influence of extrinsic elements on F_{int} could be easily included in these expressions[25,30,31], thus allowing the comparison of the simulated results with those measured in real devices. For example, the extrinsic resistances would increase the value of F_{int}.

3. RESULTS

The I–V characteristics of the HEMT and MESFET are presented in Fig. 2. The gate voltage, V_{gs}, includes the built-in potential of the Schottky contact. The thick doped layer under the gate of the MESFET supplies more carriers than that of the HEMT and so the MESFET can provide a larger drain current under the same bias conditions. The effect of the enhanced carrier mobility in the GaAs channel of the HEMT is not able to override the higher number of carriers in the channel of the MESFET. Therefore, the values of the transconductance in the MESFET are higher than those of the HEMT at high gate voltages (when this effect is more important, since the conduction takes place in almost the whole thickness of the devices). Short-channel effects, like high drain conductance and shift of the threshold voltage, are more pronounced in the

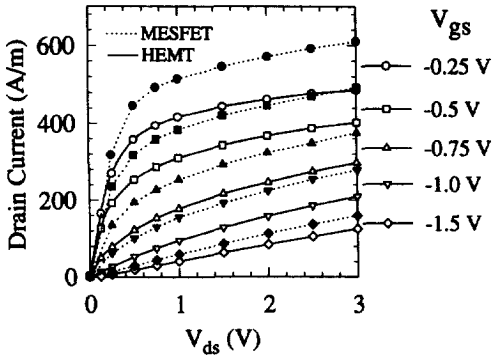

Fig. 2. I_d–V_{ds} characteristics of the MESFET (dotted line, close symbols) and HEMT (solid line, open symbols). The gate voltages include the built-in potential of the Schottky contact.

MESFET, as it can be expected in view of its lower aspect ratio. The origin of these negative effects lies in the fact that the gate potential in the MESFET is not able to control the large amount of current flowing through the substrate[32]. In this device the threshold voltage, V_T, is -3.0 V, while in the HEMT is -2.5 V (V_T is defined as the gate voltage for which the drain current vanishes, extrapolating from an $\sqrt{I_d} - V_{gs}$ curve under a drain voltage of 1.0 V). In the case of the HEMT the current is more confined in the vicinity of the heterojunction, and so the gate control is improved. This effect diminishes when the drain voltage increases, since the injection of carriers in the GaAs buffer of the HEMT becomes important. At equilibrium, the sheet electron density in the channel of the simulated HEMT is 0.9×10^{12} cm^{-2}, which is in good agreement with usual measured values[1].

Once the static behaviour of the devices is determined, the following step is the small signal characterisation. Figure 3 presents the values of g_m, g_{ds}, C_{gs}, C_{gd} and C_{ds} (these parameters are frequency independent up to 100 GHz) and current gain cut-off frequency [$f_t = g_m/2\pi(C_{gs} + C_{gd})$] for both devices as a function of the drain current (for a constant drain voltage). Under high current conditions, when the conduction takes place mainly through the layers in contact with the gate, the transconductance in the MESFET reaches larger values than in the HEMT (Figs. 3(a) and 3(b)) because of the higher electron mobility in the n layer of the MESFET with respect to that in the AlGaAs layer of the HEMT. But in the range where the variation of V_{gs} is affecting the accumulation layer of the HEMT ($V_{gs} \approx -0.75$ V, $I_d \approx 200$ A m^{-1}), g_m increases and is higher than in the MESFET, since the electrons in the HEMT accumulation layer are high-mobility carriers and consequently a slight variation of their number provides an important change of the current. The behaviour of f_t is quite influenced by g_m, and its dependence on I_d follows the behaviour previously explained for g_m, thus taking higher values in the

MESFET at high and low currents and in the HEMT at the intermediate range. It is also observed that g_{ds} is similar in both devices and takes rather high values (because of short-channel effects), which is specially troublesome under saturation conditions since low values of g_{ds} are required for having high power gain[6]. At the transconductance peak, the voltage gain (g_m/g_{ds}) in both devices is around 10 dB (which is a common value in real transistors).

In Figs 3(c) and 3(d) we notice that the most important capacitance is C_{gs} (squares) since it takes the highest values and limits the frequency behaviour of the devices. The value of C_{gs} is determined only by the variation of the source part of the gate space-charge region, while C_{gd} is a consequence of two opposite effects. The first one is the variation of the space-charge region, which has a positive

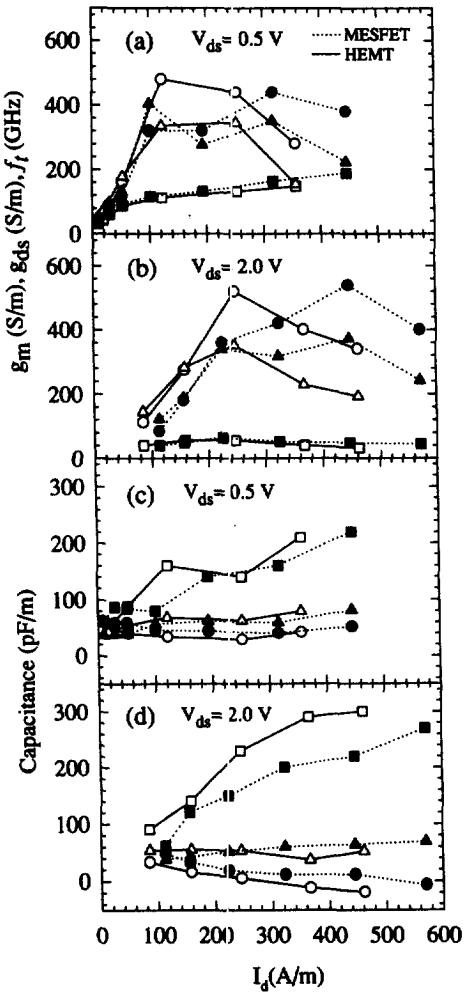

Fig. 3. Values of the transconductance, (g_m, circles), drain conductance, (g_{ds}, squares), cut-off frequency, (f_t, triangles), and capacitive elements (C_{g1}, circles, C_{gs} squares and C_{ds} triangles) of the small signal equivalent circuit for the MESFET (dotted line, close symbols) and HEMT (solid line, open symbols) as a function of the drain current for V_{ds} = 0.5 V ((a) and (c)) and V_{ds} = 2.0 V ((b) and (d)).

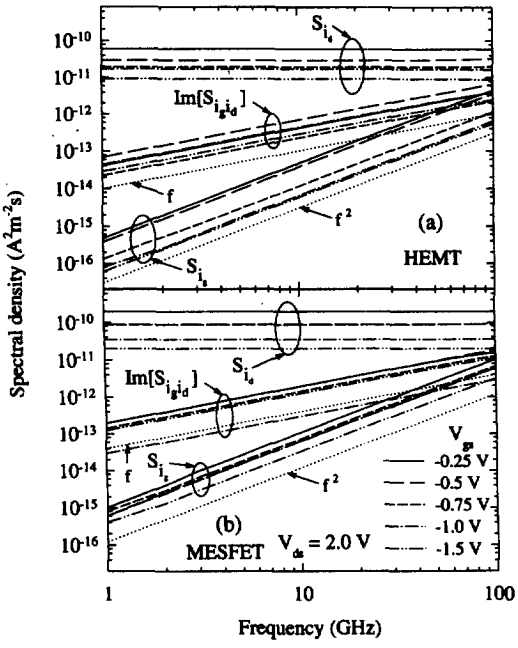

Fig. 4. Spectral density of gate- and drain-current fluctuations and its cross-correlation as a function of frequency in the saturation region, V_{ds} = 2.0 V, for different V_{gs} in the (a) HEMT and (b) MESFET. The f^2 and f dependencies are also plotted.

contribution to this capacitance (positive increment of charge with positive increment of V_{ds}). The second effect is the accumulation of carriers produced at the drain side of the gate because of the intervalley transitions, which increases with the increase of the drain potential, thus providing a negative contribution to C_{gd} (positive increment of charge with negative increment of V_{ds}). This second effect makes C_{gd} much lower than C_{gs}, which is especially evident for V_{gs} = 2.0 V (Fig. 3(d)) when intervalley transitions are very important, thus making C_{gd} take even negative values[19]. It can be appreciated that C_{gs} is higher in the HEMT, as corresponds to its narrower space charge region (because of the higher doping of the layer in contact with the gate). In the case of C_{gd}, the effect of the higher doping of the HEMT is compensated by its more important accumulation domain, which reduces this capacitance and makes it similar to that of the MESFET. Sometimes C_{gd} is neglected in the equivalent circuit[25], but in our devices this is possible only in the high-current region, since for low V_{gs} the value of C_{gd} is of the same order than that of C_{gs}. The values of C_{ds} are similar in both MESFET and HEMT, and much greater than C_{gd}. Such unusual high values of C_{ds} are caused by the pronounced short-channel effects, which make the injection of carriers into the substrate very important, leading to a notable source-drain coupling.

At this point, the noise characterisation can be performed. Firstly, the spectral density of gate- and drain-current fluctuations and its cross correlation

are calculated (S_{i_d}, S_{i_g} and $S_{i_g i_d}$, respectively). In Fig. 4 the values of S_{i_d}, S_{i_g} and $S_{i_g i_d}$ vs frequency in the saturation region of the HEMT (Fig. 4(a)) and MESFET (Fig. 4(b)) are presented. The long-time tail of the autocorrelation function of current fluctuations leads to an important uncertainty in the values of the spectral densities, mainly in S_{i_g} and $S_{i_g i_d}$, since they take very low values. Thus, following Ref. [23], the zero-frequency values of S_{i_g} and $S_{i_g i_d}$ are subtracted from $S_{i_g}(f)$ and $S_{i_g i_d}(f)$ to obtain the results shown in Fig. 4. It can be observed that in both devices S_{i_d} is constant with frequency and its value is roughly proportional to I_d. S_{i_g} shows an f^2 dependence with a proportionality factor which is also increasing with the drain current, and $\mathrm{Im}[S_{i_g i_d}]$ is proportional to f. The real part of $S_{i_g i_d}$ takes always negative (but insignificant) values, and it can be neglected[27]. These results agree satisfactorily with the conventional analysis of noise in FETs[24,25,27].

It is not possible to extract correct conclusions about the noise performance of both devices from the values of the spectral densities, since different devices with different levels of current, conductances and capacitances are compared. Anyway, the S_{i_d} values are found to be higher in the MESFET as a result of the higher drain current. For the comparison to be meaningful it is necessary to make use of normalised noise parameters providing clear information about the noise performance of the devices. The P, R and C noise parameters are adequate to this purpose. They are calculated following eqns (1)–(3). Their values vs I_d under saturation conditions ($V_{ds} = 2.0$ V) are presented in Fig. 5. No significant frequency dependence was found up to 100 GHz.

P describes the channel noise caused by velocity fluctuations, and R the gate noise induced from the channel noise[22]. In Ref. [22] a decomposition of the channel in ohmic region (linear electron velocity-field relation) and high-field region (electrons travelling with saturation velocity) is performed, and the values of the P and R parameters are calculated as the sum of the contributions from the two parts. The contribution to P from the ohmic region, which is proportional to $g_{ds}^2/g_m I_d$, is responsible for the increase of P at decreasing low currents, and the one from the high-field region, which is proportional to $g_{ds}^2 I_d/g_m$, for the increase at high currents. This typical "U-shape" dependence of the P parameter on V_{gs} (and therefore on I_d)[6,22,33] is found in the HEMT, but not in the MESFET (Fig. 5(a)), where it is observed that P does not increase at low currents. This is because of short-channel effects: the MESFET is difficult to be pinched off and so both g_m and I_d do not decrease as much as in the HEMT (g_{ds} is almost constant in both devices). The dependence of P on the drain voltage is very weak.

The calculated values for R and C (Figs. 5(b) and (c)) are not very accurate. The relative error can reach 30%, since the low frequency values of S_{i_g} and $S_{i_g i_g}$ are very small and involve a large uncertainty, as was discussed previously. Anyway, the qualitative behaviour of P, R and C agrees satisfactorily with the values extracted from experimental measurements[22,30,31] and calculated theoretically[6,28] in other HEMT structures. Thus the simulation can provide useful information on the dependence of the noise parameters on bias and allows a reliable MESFET-HEMT comparison. In Fig. 5(b) it can be observed that R decreases when V_{gs} is lowered (and consequently I_d diminishes) as a consequence of the increasing barrier imposed by the gate voltage for the electrons to approach the gate electrode. By increasing the drain voltage the electrons get enough energy to go over this barrier and move near the gate, and thus R becomes higher. Figure 5(c) shows that the correlation coefficient is nearly constant with I_d. The larger value of the HEMT aspect ratio makes C higher in this device with respect to the MESFET, with an important difference appearing mainly for a current around 200 A m^{-1}. This higher value of C means a stronger cancellation between gate and drain noise and, as we will see, leads to a lower value of the noise figure.

The most characteristic noise parameter of a given device is the minimum noise figure. Measurements usually characterise the noise behaviour of the devices with this parameter[1–3,5,28,33]. We will focus on the intrinsic value of the minimum noise figure, which is obtained in the simulation from eqns (4)–(9) (where the extrinsic elements, if known,

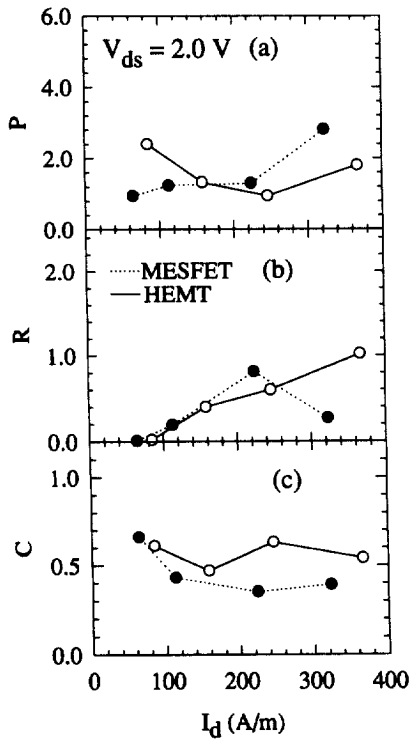

Fig. 5. (a) P (b) R and (c) C parameters of the MESFET (dotted line, close symbols) and HEMT (solid line, open symbols) as a function of I_d for $V_{ds} = 2.0$ V.

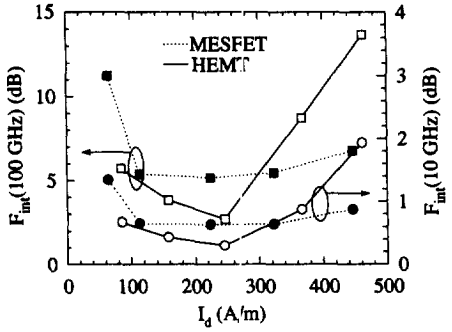

Fig. 6. F_{int} for two frequencies, 10 GHz (circles) and 100 GHz (squares), for the MESFET (dotted line, close symbols) and HEMT (solid line, open symbols) as a function of I_d for $V_{ds} = 2.0$ V.

could be included to calculate the total minimum noise figure). Figure 6 presents the dependence of F_{int} on I_d for both devices under saturation conditions (at two frequencies, 10 and 100 GHz). The typical behaviour of F_{int} can be observed: it exhibits a minimum at intermediate gate voltages and increases at both high and low currents. F_{int} is very high at large I_d because of the increase of both the drain and gate noise (P and R respectively). The noise figure is reduced as the drain current diminishes, but at very low I_d the decrease of the cut-off frequency makes F_{int} increase again[28]. The optimum operation point for the HEMT is $I_d \approx 250$ A m^{-1} ($V_{gs} \approx -0.75$ V), where F_{int} takes its minimum value (0.3 dB at 10 GHz and 2.5 dB at 100 GHz) and g_m reaches its maximum, thus providing low noise and high gain up to very high frequencies. In the case of the MESFET the optimum operation point corresponds to a higher current, $I_d \approx 400$ A m^{-1} ($V_{gs} \approx -0.5$ V), since g_m reaches its maximum at this current and F_{int} does not vary substantially at intermediate gate potentials (around 0.7 dB at 10 GHz and 5.5 dB at 100 GHz). The minimum value of F_{int} in the HEMT is lower than in the MESFET since it is reached at a lower drain current, when P and R are smaller. In addition it coincides with the maximum of g_m, which leads to a high cut-off frequency, thus showing very good noise performance up to very high frequencies. In the MESFET the most important part of the current flows near the gate, and hence g_m reaches its maximum at a higher gate potential for which the drain and gate noise are more pronounced (and its cancellation lower), leading to a higher noise figure.

In resume, concerning the P, R, and C parameters, we have not found important differences between our MESFET and HEMT devices, with these particular geometries and doping profiles. The main difference lies in the fact that the maximum current control in the HEMT is accomplished at lower drain current values than in the MESFET. This leads to a better noise performance (in terms of the intrinsic minimum noise figure) of the heterojunction devices at the optimum operation point.

4. CONCLUSIONS

A comparison between the noise performance of two particular MESFET and HEMT structures was carried out by using a Monte Carlo simulation. The behaviour of the simulated noise parameters is in good agreement with theoretical predictions and experimental measurements in HEMTs and MESFETs. Some remarkable differences were found between both devices.

(i) The maximum current control in the HEMT is accomplished when the conduction takes place through the GaAs channel, far from the gate electrode, while in the MESFET the gate control improves when the current flows near it.
(ii) The transconductance maximum in the HEMT is shifted to lower values of the current with respect to the MESFET. As a consequence, the optimum operation point of the HEMT takes place at lower drain current, thus leading to a lower gate and drain noise and hence to a lower noise figure.
(iii) While providing the same current levels, short-channel effects in the HEMT are less pronounced than in the MESFET because of its higher aspect ratio. In fact, in real HEMTs it is easier than in real MESFETs to avoid these negative effects when reducing the gate length, since their aspect ratio can be enlarged (without affecting the conducting channel) by means of a thinner cap layer.

The conclusions reached with our analysis can not be extended directly to HEMTs and MESFETs with any geometry, doping profile or material composition. The optimisation of the present structures in order to obtain better values of the transconductance and cut-off frequency could change completely the noise performance of the devices, since transconductance and noise are very closely related. However, the analysis of the influence on the noise of the different parameters and processes taking place inside the devices that has been performed can be used as an useful indicator of the differences that may be found between both types of devices.

Acknowledgements—This work was supported partially by the EC program ELEN through the contract no. ERBCHRXCT 920047, and the project TIC95-0652 from the Comisión Interministerial de Ciencia y Tecnología (CICYT).

REFERENCES

1. Whiteside, C. F., Bosman, G., Morkoc, H. and Kopp, W. F., *IEEE Trans. Electron Devices*, 1986, **ED-33**(10), 1439.
2. Joshin, K., Asai, S., Hirachi, Y. and Abe, M., *IEEE Trans. Electron. Devices*, 1989, **36**, 2274.
3. Duh, K. H. G., Chao, P. C., Liu, S. M. J., Ho, P., Kao, M. Y. and Ballingall, J. M., *IEEE Microwave and Guided Wave Lett.*, 1991, **1**, 114.
4. Mimura, T., Hiyamizu, S., Fujii, T. and Nanbu, N., *Jpn. J. Appl. Phys.*, 1980, **19**, L255.

5. Feng, M., Scherrer, D. R., Apostolakis, P. J. and Kruse, J. W., *IEEE Trans. Electron Devices*, 1996, **43,** 852.
6. Cappy, A., *IEEE Trans. Microwave Theory Tech.*, 1988, **36,** 1.
7. Jacoboni, C. and Lugli, P., *The Monte Carlo Method for Semiconductor Device Simulation*. Springer–Verlag, Vienna, 1989.
8. Mateos, J., González, T., Pardo, D., Tadyszak, P., Danneville, F. and Cappy, A., *Solid-St. Electron.*, 1996, **39,** 1629.
9. Mateos, J., González, T., Pardo, D., Tadyszak, P., Danneville, F. and Cappy, A., *IEEE Trans. Electron Devices*, accepted for its publication.
10. Fischetti, M. V. and Laux, S. E., *Phys. Rev. B*, 1988, **38,** 9721.
11. Widiger, D. J., Hess, K. and Coleman, J. J., *IEEE Electron Device Lett.*, 1984, **EDL-5,** 266.
12. Widiger, D. J., Kizilyalli, I. C., Hess, K. and Coleman, J. J., *IEEE Trans. Electron Devices*, 1989, **ED-32,** 1092.
13. Yokoyama, K. and Hess, K., *Phys. Rev. B*, 1986, **33,** 5595.
14. Brennan, K. F. and Park, D. H., *J. Appl. Phys.*, 1989, **65,** 1156.
15. González, T. and Pardo, D., *Solid-St. Electron.*, 1996, **39,** 555.
16. Jensen, G. U., Lund, B., Fjeldly, T. A. and Shur, M., *IEEE Trans. Electron Devices*, 1991, **38,** 840.
17. Mateos, J., González, T. and Pardo, D., *J. Appl. Phys.*, 1995, **77,** 1564.
18. González, T. Velázquez, J. E., Gutierrez, P. M. and Pardo, D., *Semicond. Sci. Technol.*, 1991, **6,** 862.
19. Moglestue, C., *Monte Carlo Simulation of Semiconductor devices*. Chapman & Hall, London, 1993, p. 185.
20. González, T. and Pardo, D., *IEEE Trans. Electron Devices*, 1995, **42,** 605.
21. Singh, R. and Snowden, C., *IEEE Trans. Microwave Theory Technol.*, 1996, **44,** 114.
22. Klesper, B. H., Bergamaschi, C., Schefer, M., Diskus, C. G., Patrick, W. and Bächtold, W., *IEEE Trans. Electron Devices*, 1995, **42,** 1882.
23. González, T., Pardo, D., Varani, L. and Reggiani, L., *IEEE Trans. Electron Devices*, 1995, **42,** 991.
24. van der Ziel, A., *Proc. IRE*, 1963, **51,** 461.
25. Pucel, R. A., Haus, H. A. and Statz, H., *Adv. Electr. Electron Phys.*, 1975, **38,** 195.
26. Danneville, F., Dambrine, G., Happy, H., Tadyszak, P. and Cappy, A., *Solid-St. Electron.*, 1995, **38,** 1081.
27. Danneville, F., Happy, H., Dambrine, G., Belquin, J. M. and Cappy, A., *IEEE Trans. Electron Devices*, 1994, **41,** 779.
28. Cappy, A., Vanoverschelde, A., Schortgen, M., Versnaeyen, C. and Salmer, G., *IEEE Trans. Electron Devices*, 1985, **32,** 2787.
29. Rothe, H. and Dahlke, W., *Proc. IRE*, 1956, **44,** 811.
30. Greaves, S. D. and Unwin, R. T., *Microwave and Opt. Tech. Lett.*, 1993, p. 60.
31. Taylor, R. I., Brookbanks, D. M. and Holden, A. J., *Electron. Lett.*, 1991, **27,** 1923.
32. Awano, Y., Kosugi, M., Kosemura, K., Mimura, T. and Abe, M., *IEEE Trans. Electron Devices*, 1989, **36,** 2260.
33. Duh, K. H. G., Liu, S. M. J., Lester, L. F., Chao, P. C., Smith, P. M., Das, M. B., Lee, B. R. and Ballingall, J. M., *IEEE Electron. Dev. Lett.*, 1988, **9,** 521.